Intramolecular hydrogen migration in Alkylperoxy and Hydroperoxyalkylperoxy radicals: Accurate treatment of hindered rotors

Citation: Sharma, Sandeep, Sumathy Raman, and William H. Green. "Intramolecular Hydrogen Migration in Alkylperoxy and Hydroperoxyalkylperoxy Radicals: Accurate Treatment of Hindered Rotors." The Journal of Physical Chemistry A 114.18 (2010): 5689-5701.

As Published: http://dx.doi.org/10.1021/jp9098792

Publisher: American Chemical Society

Persistent URL: http://hdl.handle.net/1721.1/49493

Version: Author's final manuscript: final author's manuscript post peer review, without publisher's formatting or copy editing

Intramolecular hydrogen migration in Alkylperoxy and Hydroperoxyalkylperoxy radicals: Accurate treatment of hindered rotors.

Sandeep Sharma[a]; Sumathy Raman[b]; William H. Green[a*]

[a] *Department of Chemical Engineering, Massachusetts Institute of Technology, Cambridge, Massachusetts 02139, USA*

[b] *ExxonMobil Research and Engineering Company, 1545 Route 22 East, Annandale, NJ 08801, USA*

September 15, 2009

Abstract

We have calculated the thermochemistry and rate coefficients for stable molecules and reactions in the title reaction families using CBS-QB3 and B3LYP/CBSB7 methods. The accurate treatment of hindered rotors for molecules having multiple internal rotors with potentials that are not independent of each other can be problematic and a simplified scheme is suggested to treat them. This is particularly important for hydroperoxyalkylperoxy radicals (HOOQOO). Two new thermochemical group values are suggested in this paper and with these values the group additivity method for calculation of enthalpy as implemented in RMG gives good agreement with CBS-QB3 predictions. The barrier heights follow the Evans-Polanyi relationship for each type of intramolecular hydrogen migration reaction studied.

1 Introduction

Recently, there has been an increasing interest in improving the efficiency and lowering the emissions from operating combustors, e.g. internal combustion (IC) engines and gas turbines. Many researchers in the automotive industry are studying combustion in a new type of IC engines known as homogeneous charge compression ignition (HCCI) combustion,[1] which is a very promising research direction. This type of combustion happens at low temperature under lean or stoichiometric conditions, and thus the NOx is lower than in conventional IC engines and soot emissions are lower than in diesel engines. The high CO and hydrocarbon emissions and also the instability of combustion are serious challenges in these engines. In order to make progress in these areas, a fundamental understanding of the low temperature combustion chemistry must be developed.

At low temperatures (< 900 K) most alkanes undergo combustion via the formation of chemically activated alkylperoxy (RO_2) radicals. The RO_2 can undergo intramolecular-H-migration resulting in the formation of a hydroperoxyalkyl radical (QOOH). QOOH with

Corresponding author: whgreen@mit.edu

the hydroperoxy group β to the radical center can β-scission to olefin + HO_2. A direct concerted pathway resulting in the formation of olefins and HO_2 from RO_2 was elucidated by Kiracofe et al.[2] in ethane oxidation. Here the barrier for concerted elimination of HO_2 is about 5 kcal/mole lower than the intramolecular-H-migration with a 5-membered-ring transition state resulting in the formation of CH_2CH_2OOH.[3] In higher alkanes the intramolecular-H-migration is competitive with the concerted HO_2 elimination due to the larger size of the rings in transition states and also due to the presence of secondary and tertiary H atoms which are easier to abstract. QOOH thus formed can have many fates, including the formation of olefins and HO_2, cyclic ethers and OH[4] and addition of another O_2 molecule resulting in the formation of OOQOOH. OOQOOH can also undergo intramolecular-H-migration, where in many cases the most favourable reaction is migration of a H atom on the carbon atom α to the OOH group, resulting in the formation of OH and ketohydroperoxide. Under most conditions the weak O–O bond in the resulting ketohydroperoxide eventually fragments into 2 radicals; this sequence is a major source of free radicals at low temperatures (700 K).

Direct measurements of the reaction rates of intramolecular-H-migration in ROO and OOQOOH are challenging and the rate coefficients can only be inferred indirectly from experiments. Walker et al.[5–10] in their pioneering work have introduced a variety of alkanes into a slowly reacting mixture of H_2 + O_2. These alkanes react with H and OH of the reacting mixture to form alkyl radicals. The alkyl radicals then go on to react with O_2 molecules to form products. By studying these products they were able to infer the rate coefficients of various reactions including intramolecular-H-migrations in some RO_2 radicals. More recently spectroscopic experiments were performed by Taatjes et al.[11–15] in which alkyl radicals are generated by pulsed laser photolysis of alkyl halides which directly form alkyl radicals or photolysis of Cl_2 which form Cl radicals that react with alkanes to form alkyl radicals. These alkyl radicals then react with oxygen to form products. The time profile of HO_2, OH and halogen atoms formed during the reaction is measured using probe lasers. Kaiser et al.[16–19] performed similar experiments but instead of time-resolved measurements they measured product yields. These experiments usually do not directly give rate coefficients of reactions, but are used in concert with theoretical calculations to get insight into mechanisms and rate coefficients.[20–23]

Several intramolecular-H-migrations of ROO and OOQOOH radicals have been studied theoretically including ethyl + O_2,[2,3,24–27] propyl + O_2,[13,21,22,28–30] butyl + O_2[20,31,32] and neopentyl + O_2.[33–36] Chan et al.[37] have studied the structure reactivity relation for intramolecular-H-migration for various ROO species using BH&HLYP methods. To our knowledge Chan's[37] is the first systematic study of this reaction family using quantum mechanical methods although the level of theory used is not very accurate and also they failed to take into account the effect of hindered rotors leading to significant errors in the reported A factors. Intramolecular-H-migration in ROO has also been studied theoretically by Pfandtner et al.[38] for a series of molecules in condensed phase using the B3LYP/6-311G(d,p) method. In the present study we calculate the rate of intramolecular-H-migration for several ROO and OOQOOH radicals with different but representative structures of R and Q. These results can be generalized into rate rules needed to construct large reaction mechanisms.

2 Theoretical Methodology

All the density functional and molecular orbital calculations were performed using the Gaussian03 suite of programs.[39] All the molecules and transition state geometries and harmonic frequencies are calculated using the CBS-QB3 compound method[40–42] which calculates the energy to a complete basis set limit using empirical corrections. We have also performed calculations using the G2 method and the MP2/6-311+G(3df,2p) method. G2[43] is another compound method which uses empirical corrections to calculate the energies with reported average errors below 2 kcal/mole.

The output from the quantum chemical methods are used in conjunction with the rigid rotor harmonic oscillator approximation with corrections for hindered rotors to calculate the heats of formation, entropies and heat capacities for all the molecules. Vibrations corresponding to torsions about a single bond are treated as hindered rotors. For hindered rotors a relaxed scan was performed with dihedral angle increments of 30^o using B3LYP/6-31G(d) and this potential was fit to a Fourier series of the form $V(\phi) = A_0 + \sum_{m=1}^{5} A_m \sin(m\phi) + B_m \cos(m\phi)$. The potential was used to solve the one dimensional Schroedinger equation in ϕ to calculate the energy levels and consequently the partition function of the hindered rotor. The $I^{(2,3)}$ [44] reduced moment of inertia evaluated at the equilibrium geometry was used in the 1-D Schroedinger equations. This approach of treating hindered rotors implicitly assumes that the potential V at a set of dihedral angles ϕ_is

$$V(\phi_1, \phi_2, ..\phi_n) = V_1(\phi_1) + V_2(\phi_2) + ... + V_n(\phi_n) + V^{ref}(\phi_1^{ref}, .., \phi_i^{ref}, .., \phi_n^{ref}) \qquad (1)$$

can be written as a sum of independent contributions for each dihedral angle ϕ_i, where

$$V_i(\phi_i) = V^{ref}(\phi_1^{ref}, .., \phi_i, .., \phi_n^{ref}) - V^{ref}(\phi_1^{ref}, .., \phi_i^{ref}, .., \phi_n^{ref}) \qquad (2)$$

The superscript ref, on ϕ_i denotes that the angle has the same value as in reference geometry and on V denotes the energy of the reference geometry with respect to the lowest energy conformer. Speybroeck et al.[45,46] have shown that this approach of treating the hindered rotors is satisfactory for normal alkanes. We examine the validity of this approach for treating hydroperoxyalkylperoxy radicals and suggest improved methods in Section 3.3.

In all hydroperoxyalkylperoxy radicals studied in this paper the oxygen atoms interact with hydrogen atoms. This interaction results in a lowest energy conformer that has a ring shape with the peroxyl group forming a hydrogen bond with the OOH group. To calculate the absolute minimum conformer we change dihedral angle for each rotor by 120^o to get the initial guess and then start the optimization from this guess using B3LYP/6-31G(d) method. So for example, $HOOCH_2CH_2OO$ has 4 rotors and we generate $(360/120)^4 = 81$ initial guesses of conformer geometries and then optimize all these initial guesses to find the minimum energy conformer. We do not perform the complete conformational analysis for molecules which are derived from straight chain molecule by having methyl side chains (e.g. $HOOCH(CH_3)CH_2OO$). Instead, we take the six lowest energy conformers of the corresponding straight chain molecule and add the methyl radicals at the required positions. These six geometries are taken as initial guesses and are optimized using B3LYP/6-31G(d) method. The lowest energy conformers obtained in this fashion are then used to calculate the CBS-QB3 energies.

For long chain molecules having many hindered rotors, some of these hindered rotations do not correspond to any of the normal vibrational modes. In other words the low frequency vibrations of the molecules include mixing of various hindered rotations and other vibrations. For such molecules, which low frequency vibrational modes to replace with hindered rotors becomes subjective and causes some uncertainty in the thermochemistry and rate constant calculations. To overcome this problem we remove the projection of the force constant matrix along the vectors corresponding to hindered rotors. When the resulting force constant matrix is diagonalized it contains only $3N-6-d$ non-zero eigenvalues, where N is the number of atoms in the molecule and d is the number of hindered rotors. This approximation provides a unique separation of the internal rotors from the small amplitude vibrations.

Let v_1 and v_2 be the coordinates of the two pivot atoms 1 and 2 respectively about which torsional rotation is happening. Let $v_{11}, v_{21}, ..., v_{n1}$ be the coordinates of all the atoms on the rotating group attached to the pivot atom 1 and $v_{12}, v_{22}, ..., v_{m2}$ be the coordinates of all the atoms in the rotating group attached to the pivot atom 2. Then the torsional coordinate is given in cartesian coordinate by the vector s in Equation 3.

$$s = \begin{pmatrix} \frac{(v_{11}-v_1)\times(v_1-v_2)}{|v_1-v_2|} \\ \vdots \\ \frac{(v_{n1}-v_1)\times(v_1-v_2)}{|v_1-v_2|} \\ \frac{(v_{12}-v_2)\times(v_2-v_1)}{|v_2-v_1|} \\ \vdots \\ \frac{(v_{m2}-v_2)\times(v_2-v_1)}{|v_2-v_1|} \end{pmatrix} \tag{3}$$

In addition to these d torsional vectors s_i we also calculate 3 translational vectors t_i and 3 external rotational vectors r_i by the usual formulas.[47] These vectors s_i, t_i and r_i are then used to form a set of orthonormal vectors o_i which span the same space as the $6+d$ original vectors. A matrix $O = [o_1 o_2 .. o_{6+d}]$ of size $(3N, d+6)$ is then used to generate the projection matrix $P = OO^T$. The new force constant matrix K,[48]

$$K = (I-P)F(I-P)$$

has $3N-6-d$ non-zero eigenvalues and the eigenvectors corresponding to non-zero eigenvalues are orthogonal to the hindered rotation vectors s_i. The $3N-6-d$ vibrational frequencies can then be calculated by evaluating the force constant matrix K in mass-weighted cartesian coordinates and performing eigenvalue analysis on the resulting matrix.[47] Note that Speybroeck et al.[49] have recently recommended a different method for dealing with this problem as discussed in Section 3.3.

The frequencies calculated using B3LYP/CBSB7 method which are used in CBS-QB3 calculations are corrected using a factor of 0.99 as recommended by Scott et al.[50] Bond group additivity correction (BAC) as prescribed by Petersson et al.[51] was used to calculate heats of formation.

To calculate the high-pressure-limit rate constants for the reactions we have used canonical transition state theory. The transition states themselves have torsional modes which have been separated out and have been treated as hindered rotors as described earlier. Finally, the rate constants are corrected using the simple Wigner tunneling correction.[52]

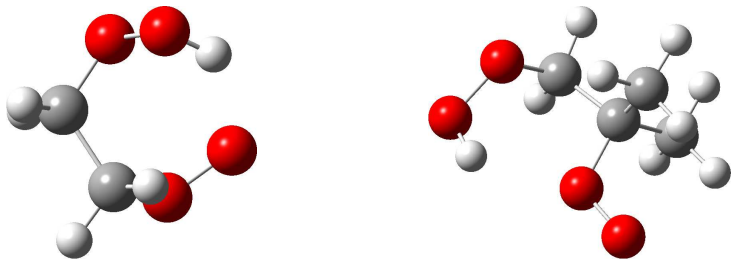

(a) $HOOCH_2CH_2OO$ (b) $HOOCH_2C(CH_3)_2OO$

Figure 1: The lowest energy conformers of two OOQOOH radicals.

3 Results and Discussion

We first discuss the result of the conformational analysis that we have performed to calculate the lowest energy conformer for each hydroperoxyalkylperoxy radical. We follow this with a discussion of the accuracy of various quantum chemistry methods for the system under study and the correct way of treating hindered rotors. Based on these two sections we select a quantum chemical method and appropriate treatment of the hindered rotors to calculate the rate coefficients and thermochemistry of the pertinent reactions and molecules respectively. The trends in the rate constants and thermochemistry are discussed and the values are tabulated for easy use in chemical kinetics mechanisms.

3.1 Lowest Energy Structure

For hydroperoxyalkylperoxy radicals the lowest energy structures is not a straight chain conformer but instead a ring in which the oxygen atoms form hydrogen bonds.

Predicting the lowest energy conformer *a priori* is difficult, which is demonstrated here by the lowest energy conformers for $HOOCH_2CH_2OO$ and $HOOCH_2C(CH_3)_2OO$ computed at the CBS-QB3 level, which have different patterns of hydrogen bonds, shown in Figure 1. The geometries of the lowest energy conformers found in this work are detailed in the Supporting Information.

3.2 Comparison of Quantum Methods

3.2.1 Intramolecular-H-migration in ROO

To compare the barrier heights and saddle point geometries computed by different methods for $RO_2 \rightarrow QOOH$, we studied $CH_3CH_2OO \rightarrow CH_2CH_2OOH$ and $CH_3CH_2CH_2OO \rightarrow CH_2CH_2CH_2OOH$.

As mentioned in Section 1 Pfaendtner et al.[38] have studied a series of reaction rates for intramolecular-H-migration in ROO radicals in solution phase. From their study they found that the CBS-QB3 compound method predicted activation energies with an error of less than 1.5 kcal/mole compared to solution phase experimental values,[53–55] which were back calculated by authors based on measured rate coefficients at different temperatures. Table 1 shows that the difference between the barrier heights predicted by CBS-QB3 and G2 methods for $CH_3CH_2OO \rightarrow CH_2CH_2OOH$ and $CH_3CH_2CH_2OO \rightarrow$

Method	Transition State				$\Delta E_0+\Delta ZPE$
	E_0+ZPE (a.u.)	C–H (Å)	O–H (Å)	ν (cm^{-1})	(kcal/mole)
$CH_3CH_2OO \rightarrow CH_2CH_2OOH$					
CBS-QB3	-229.1332	1.391	1.198	$2273i$	35.9
DFT	-229.4708	1.391	1.198	$2273i$	37.8
MP2	-228.8324	1.281	1.251	$2856i$	40.2
G2	-229.1161	1.298	1.249	$3316i$	38.4
$CH_3CH_2CH_2OO \rightarrow CH_2CH_2CH_2OOH$					
CBS-QB3	-268.3648	1.406	1.154	$1637i$	23.4
DFT	-268.7736	1.406	1.154	$1637i$	24.3
MP2	-268.0622	1.284	1.213	$2037i$	26.1
G2	-268.4021	1.304	1.210	$3170i$	25.6

Table 1: Transition state properties and barrier heights for the reactions $CH_3CH_2OO \rightarrow CH_2CH_2OOH$ and $CH_3CH_2CH_2OO \rightarrow CH_2CH_2CH_2OOH$. MP2 represents MP2/6-311+G(3df,2p) and DFT represents B3LYP/6-311+G(3df,2p) methods. E_0+ZPE is the electronic plus zero point energy in units of hartree, C–H is the breaking carbon hydrogen bond length, O–H is the forming oxygen hydrogen bond length and ν is the imaginary frequency.

$CH_2CH_2CH_2OOH$ are 2.5 kcal/mole and 2.2 kcal/mole respectively which is a little on the high side but not very surprising given the fact that both these methods are known to have accuracy of around 2 kcal/mole for stable molecules. As is also the case for intramolecular-H-migration in OOQOOH the barrier height predicted by MP2 method is higher than the CBS-QB3 method by about 3-4 kcal/mole. The barrier height predicted by B3LYP method is also higher than that of CBS-QB3 method although by only about 2.1 kcal/mole and 0.9 kcal/mole for the two cases respectively. In Section 3.5.4 we compare the CBS-QB3 results with values taken from literature and the comparisons are quite good.

3.2.2 Intramolecular-H-migration in OOQOOH

The key reaction leading to chain-branching (one radical becoming 3 radicals) is H-migration from the carbon attached to the OOH group to the peroxyl radical site. To compare the barrier-heights predicted by various ab-initio methods, CBS-QB3, B3LYP/6-311+G(3df,2p), G2 and MP2/6-311+G(3df,2p) calculations on the reactant and transition state of Reaction 1 were performed. The results of the calculations are displayed in Table 2. Notice in this reaction we have written products as $HOOCH_2CHO$ + OH instead of just $HOOCHCH_2OOH$ and this point is discussed in detail later.

$$OOCH_2CH_2OOH \rightarrow HOOCH_2CHO + OH \quad (1)$$

Table 2 shows that the barrier height predicted by MP2 method is more than 5 kcal/mole different than the rest of the methods which are all very similar to each other. It is interesting to note that although the DFT method over predicts the barrier height compared to the CBS-QB3 method for intramolecular-H-migration in ROO radical it agrees

Method	Transition State					$\Delta E_0+\Delta ZPE$
	E_0+ZPE (a.u.)	C–H (Å)	O–H (Å)	ν (cm^{-1})	O–O (Å)	(kcal/mole)
CBS-QB3	-379.3342	1.343	1.257	$1959i$	1.450	29.5
DFT	-379.8570	1.343	1.257	$1959i$	1.450	29.4
MP2	-378.8716	1.266	1.309	$2823i$	1.446	35.3
G2	-379.3048	1.300	1.283	$3175i$	1.467	29.6

Table 2: Transition state properties and barrier heights for the reaction $OOCH_2CH_2OOH \rightarrow HOOCH_2CHO + OH$. MP2 represents MP2/6-311+G(3df,2p) and DFT represents B3LYP/6-311+G(3df,2p) methods. E_0+ZPE is the electronic plus zero point energy in units of hartree, C–H is the breaking carbon hydrogen bond length, O–H is the forming oxygen hydrogen bond length, O–O is the breaking oxygen oxygen bond and ν is the imaginary frequency.

quite well with the CBS-QB3 method for intramolecular-H-migration of OOQOOH. This suggests that the presence of OOH structure on the carbon atom losing a hydrogen atom causes some cancellation of errors resulting in accurate prediction of barrier heights.

The geometries predicted by the three methods G2, MP2 and DFT (CBS-QB3 uses the geometry of DFT) are quite different. To see the effect of the geometry on the energies we have first performed IRC calculations using the B3LYP/6-31G(d) and MP2/6-311+G(3df,2p) methods. The trajectory of the IRC method is displayed in Figure 2 in terms of the breaking C–H and forming O–H bond lengths in the transition states. Along each IRC trajectory we calculate single point CBS-QB3 energies as recommended by Malick et al.[56] in their paper describing IRC-MAX calculations. The results of these calculations are presented in Figure 2. The MP2 trajectory is shifted from the B3LYP trajectory to the right by roughly 0.1 Å i.e for any given O–H bond length the C–H bond length in the MP2 trajectory is shorter than the C–H bond in B3LYP trajectory by about 0.1 Å. The barrier heights along both the trajectories are the same even though the geometries for which the maximum is obtained is quite different, in particular the C–H and O–H bond lengths for the maximum along MP2 trajectory are 1.289 Å and 1.155 Å respectively and along B3LYP trajectory are 1.337 Å and 1.396 Å respectively. This finding suggests the CBS-QB3 potential in the vicinity of the saddle point is relatively flat (note that the barrier heights in Figure 2 are very different than the value of 29.5 kcal/mole in Table 2 because the figure does not include the zero point energy difference of transition state and the reactant). Throughout the rest of the paper, unless otherwise specified, the rate coefficients for intramolecular-H-migration in OOQOOH radicals are calculated using barrier heights obtained from the CBS-QB3 method.

3.2.3 Instability of α-hydroperoxyalkyl radicals

Previously in the literature[25] it has been reported that the 1,3-hydrogen migration reaction in ROO radicals results in an unstable α-QOOH molecule where the O–O bond breaks spontaneously and we are left with the product QO + OH. In this work we were able to find geometries for some α-QOOH radicals that are local minima on the B3LYP/6-311+G(3df,2p) and B3LYP/6-31G(d) potential energy surfaces. These radicals are only

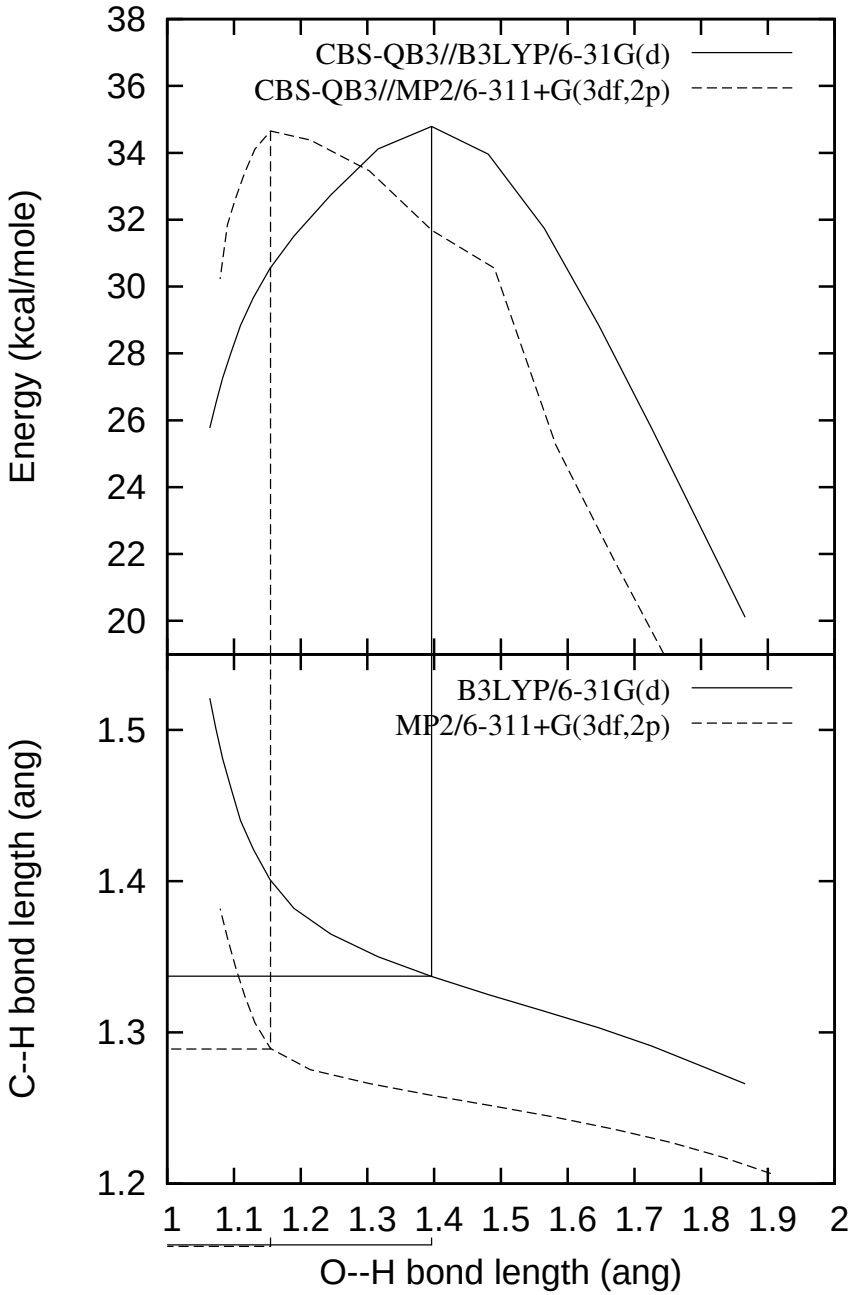

Figure 2: Results of the IRC-MAX calculations CBS-QB3//B3LYP/6-31G(d) and CBS-QB3//MP2/6-311+G(3df,2p) for Reaction 1. The lower graph shows the trajectories of the two IRCs and the upper graph shows the energy barriers calculated using CBS-QB3 along these IRC trajectories. The energies in the upper graph are electronic energies and do not include zero point energy.

weakly bound and would quickly break apart to form ketone/aldehyde + OH with a low barrier for the reaction.

On the other hand the 1,4 intra-H-migration of $HOOCH_2CH_2OO$ does not seem to form a stable α-hydroperoxyalkyl product. Figure 3 shows the IRC calculation performed at B3LYP/6-31G(d) level of theory. At this level of theory there is no minima at the $HOOCHCH_2OOH$ which goes on to lose a OH fragment to form $HOOCH_2CHO$ + OH. But when we perform optimization of $HOOCHCH_2OOH$ structure using MP2/6-311+G(3df,2p), we obtain a minimum suggesting that it is a stable molecule on the MP2/6-311+G(3df,2p) potential energy surface. The instability or metastability of α-hydroperoxyalkyl radicals has been noted several times in the literature[24,57]

To resolve the issue of the stability of α-hydroperoxyalkyl and α-hydroperoxyalkylperoxy radicals one would have to perform optimization using a higher level method which is outside the scope of the present paper. Even if these structures turn out to be a local minima they are probably very shallow minima and we expect the O–O bond to quickly break. Based on this reasoning and due to lack of more conclusive finding we recommend that kinetic models need not include α-hydroperoxyalkyl and α-hydroperoxyalkylperoxy as a kinetically significant species and only include the bimolecular product following the fission O–O bond. Note that because the α-QOOH are not expected to live long enough to react with O_2, kinetic models can also safely omit α-hydroperoxyalkylperoxy radicals formed by α-QOOH + O_2.

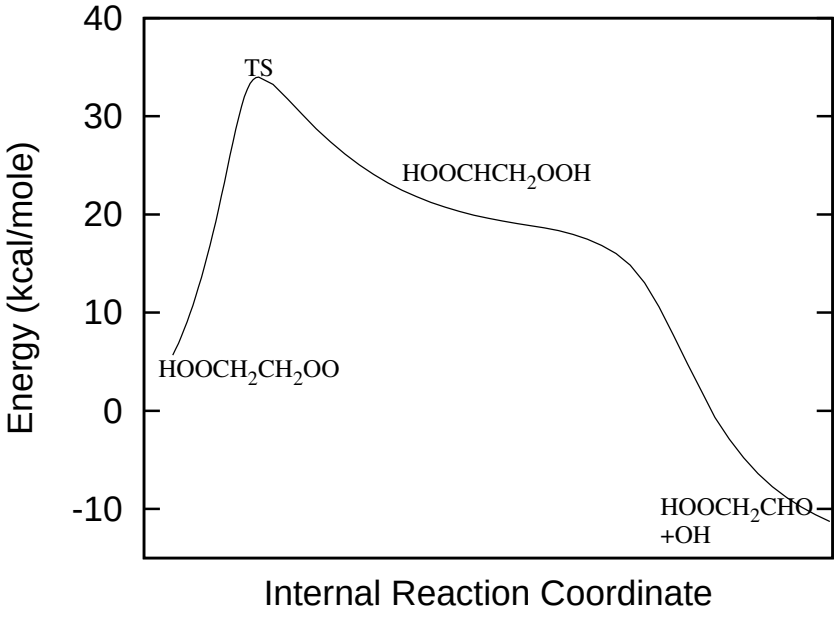

Figure 3: The potential energy surface along the reaction coordinate computed at B3LYP/6-31G(d) level. The approximate locations of various structures are shown on the figure. At this level of theory there is no local minimum near the $HOOCHCH_2OOH$ structure.

3.3 Improved Methods for Treatment of Hindered Rotors

3.3.1 Alternative method for separating rotors from normal modes

As explained in Section 2 the projection of the force constant matrix along the vectors corresponding to the internal rotations are removed. The resulting force constant matrix is used to calculate the vibration that are orthogonal to the internal rotations and these frequencies are treated as harmonic oscillators. To check the accuracy of this way of calculating the partition function and thermodynamic quantities we compare the results obtained for the molecule $HOO(CH_2)_5OO$, with that obtained when one uses the alternative method proposed by Speybroeck et al.[49] and later used by Welz et al.[58] shown in Equation 4.

$$Q_{int} = Q_{HO} \prod_{i=1}^{m} \frac{q^*_{HIR,i}}{q^*_{HO,i}} \tag{4}$$

In this equation Q_{HO} is the partition function of all the internal modes (including torsions) calculated by treating them all as harmonic oscillators, $q^*_{HIR,i}$ is the partition function calculated by solving 1-D Schroedinger equation for the i^{th} internal rotation and $q^*_{HO,i}$ is the partition function calculated by fitting $V(\phi_i)$ to a parabola and approximating the internal rotational mode as a harmonic oscillator. The superscript * is used to signify that none of these modes are normal modes. The difference in partition function between Speybroeck et al.'s method and our method described in Section 2 is less than a factor of 2 for all temperatures and the calculated entropy contribution of all the internal modes differs by about 0.5 cal/mole/K. This gives us confidence that either approach for calculating the partition function and thermodynamic quantities of molecules with hindered rotors, when the rotors are assumed to be independent of each other, is reasonable.

3.3.2 Coupled internal rotors

For molecules with multiple hindered rotors, each hindered rotor is usually treated independently and then the entropy, heat capacity and thermal correction contribution for each of them is added to get the total values. This approach effectively assumes that the potential of n different torsional modes is just the sum of each torsional mode (see Equation 1). In hydroperoxyalkylperoxy radicals this approximation is not valid because there are local minima where a combination of the different torsional angles ϕ_i give rise to a hydrogen bond. Because the torsional mode potentials are actually not independent of each other, which conformer is used to perform the hindered scans can lead to very different thermodynamic contributions from the rotors. For example, using the conventional independent rotor approach, the thermodynamic properties of $HOOCH_2CH(CH_3)OO$ are predicted to be very different (see Table 3) depending on whether the scans are performed starting from the reference geometry of the lowest energy ring conformer (Ring-Sep) or from the reference geometry of a straight chain conformer (Open-Sep).

Since the large discrepancy between the Ring-Sep and Open-Sep calculations indicate the potential is not separable, we computed Q without making the separability assumption, Equation 5.[59] For simplicity we only calculate the partition function and thermodynamic properties of the four rotors along the main chain of the molecule (i.e. we omit the methyl rotor because it is essentially independent of other rotors). In this

work we have taken $[D]$ as the product of the reduced moments of inertia $I^{2,3}$ for each of the hindered rotors.

$$Q_{int,rot} = \frac{1}{\sigma_{int}} \left(\frac{2\pi k_b T}{h^2} \right)^{n/2} [D]^{1/2} \int_{\phi_1..\phi_n} \exp\left(\frac{-V(\phi_1, \phi_2, ..\phi_n)}{k_b T} \right) d\phi_1..d\phi_n \quad (5)$$

To calculate the multi-dimensional integral we need the value of the potential $V(\phi_1, \phi_2, ..\phi_n)$ for different values of ϕ_i. To do this we have performed 12^4 single point B3LYP/6-31G(d) calculations where 12 grid points are placed on each torsional angle with a uniform grid spacing of 30^o each. Once the potential at each grid point is obtained we need a way to estimate the potential at any given arbitrary combination of ϕ_is. To do this we have tried two different approaches, four dimensional linear interpolation and four dimensional cubic splines. The expression for the four dimensional linear interpolation is given in Equation 6. The name linear can be misleading because the interpolating polynomial is only linear with respect to each coordinate but can have products of linear terms of different coordinates e.g. $C\phi_1\phi_2\phi_3\phi_4$.

$$V(\phi_1, \phi_2, ..\phi_n) = \sum_{i_1,..i_n=0}^{1} V_{i_1,..,i_n} \prod_{j=1}^{n} b_{i_j}(x_j) \quad (6)$$

In Equation 6 each index $i_1, ..i_n$ corresponds to a different coordinate and can take values of 0, which corresponds to the grid point in that particular coordinate just before the point of interest, or 1 which is the grid point just after the point of interest. The values of $x_j = (\phi_j - \phi_{j_0})/(\phi_{j_1} - \phi_{j_0})$, where ϕ_{j_0} and ϕ_{j_1} are the grid points before and after the point ϕ_j. For the case of linear interpolation, function $b_0(x_j) = (1 - x_j)$ and $b_1(x_j) = x_j$. This interpolation passes through all the grid points but may not have continuous first derivatives at these grid points. Thus for example at an energy minimum, in one dimension we see a sharp angle instead of a smooth parabolic curve. We have also tried using cubic splines, this interpolation is third order in each coordinate and is smooth at the grid points giving a more realistic description of energy minima. The down side of cubic splines is that it gives unphysical results close to points of very high energy, like the ones arising due to steric hindrance at certain dihedral angles. In order to remain smooth near these points the polynomial goes through local a minimum before rising in value to reach the high energy point. These local minima are not present in reality and can have very low energies, specially if the energy rise due to steric hindrance is high. These artifacts of fitting can lead to unphysical results and hence we have decided to use linear interpolation instead of the cubic splines for the purposes of this study.

Once we can obtain a value of V at various dihedral angles we still need to calculate the multi-dimensional integral in Equation 5. In our experience the simple Monte-Carlo method for calculating this integral is quite inefficient. For this case of 4 dihedral angles we have decided to instead use the multi-dimensional version of the rectangle rule. To do this we divide each dihedral angle into 100 smaller subdivisions, calculate the value of integrand at the center of all the 100^4 hypercubes and add up all these values to calculate the integral. The values of entropy, heat capacity and thermal correction due to the four hindered rotors calculated using this method are given in Table 3 as "Insep", along with

Method	Entropy (cal/mole/K)	Enthalpy (kcal/mole)	Cp (cal/mole/K)
Ring-Sep	9.94	2.66	13.03
Open-Sep	18.07	5.78	11.28
Insep	10.04	3.35	19.45
Piece-sep	12.34	3.26	22.06

Table 3: Thermodynamic contribution of the four hindered rotors in $HOOCH_2CH(CH_3)OO$ at 298 K computed using 4 different methods. Ring-Sep and Open-Sep represent the ordinary separable-rotors approximation of Section 2, using ring and straight chain reference conformers respectively. Insep does not assume the rotor potentials are separable Equation 5. Piece-sep assumes potential is separable only in local regions, each using different reference conformers, Equations 8.

the values calculated using the separable rotors approximation starting from different reference conformers.

Table 3 shows that the thermodynamic contributions computed using the conventional separable-rotors approximation and solving the 1-D Schroedinger equations are poor approximations to the values calculated using configurational integral without making the separable-rotors approximation. To see the difference more clearly we plot the sum of states of the four rotors in Figure 4. The classical sum of states is given as a configurational integral and for the cases of four rotors is given in Equation 7.

$$\begin{aligned} W_{cl}(E) &= \frac{1}{h^n}\int_{\phi_1,..,p_1,..} H\left(E-\mathcal{H}(\phi_1,..,p_1,..)\right) d\phi_1...dp_1.. \\ &= \left(\frac{2\pi}{h^2}\right)^{n/2}\frac{[D]^{1/2}}{\Gamma(n/2+1)}\int_{\phi_i,..}\left(E-V(\phi_1,..)\right)^{n/2} H\left(E-V(\phi_1,..)\right) d\phi_1... \quad (7) \end{aligned}$$

Figure 4 shows that the sum of states calculated using the interpolated B3LYP/6-31G(d) potential labeled Insep has an inflection point near 5 kcal/mole. This inflection point arises because as one goes up in energy at about 5 kcal/mole above the lowest energy conformer many different local potential minima become available which increases the density of states. In case of Open-sep there are many different local minima close to the energy of the starting straight-chain conformer (when individual rotor scans are performed starting from the straight chain conformer we do not encounter the global minimum ring conformer). In the Ring-sep case, the approximate sum of separable rotors potential used grossly overestimates the energies of many conformers, so it underestimates the number of states.

The Insep method presented here is more accurate than either of the conventional approaches, but it is too computationally demanding to be practical for systems with longer chains (it scales exponentially with the number of coupled internal rotors). We therefore develop another method with better scaling properties. Based on this figure we have decided it is appropriate to divide the dihedral angle phase space into two parts, one called region $\mathcal{A}$ near the global minimum and the rest of the phase space called region $\mathcal{B}$.

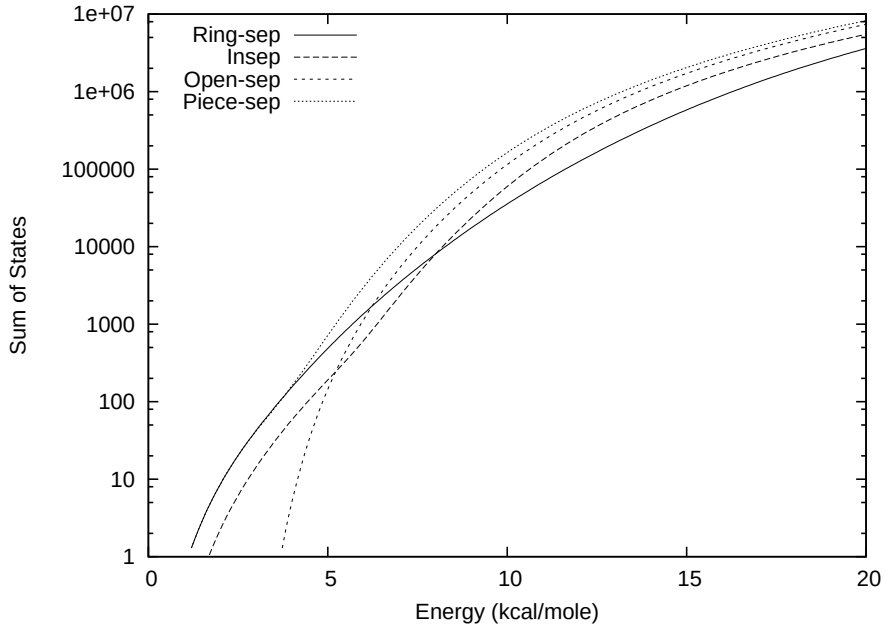

Figure 4: The sum of states of the four rotors in $HOOCH_2CH(CH_3)OO$ (all except the methyl rotors) calculated using various methods. Ring-sep represents the method in which the potential is assumed separable and is calculated using the potential scans performed starting from the most stable ring conformer. For Open-sep the potential is assumed separable and is calculated using the potential scans performed starting from a straight chain conformer. For Insep the potential is assumed non-separable and is calculated using fourth dimensional linear interpolation of the energy grid calculated using B3LYP/6-31G(d). For Piece-sep the potential is approximated by different fourier fit potentials in different regions of configurational space, each treated as separable (see text).

In region $\mathcal{A}$ we calculate the potential using information gathered from the ring shaped global minimum conformer. This information can come from dihedral scans performed on the ring conformer or can come from the normal mode analysis that will attempt to fit the potential around the local minimum to a quadratic form. In this work we used. For region $\mathcal{B}$ we use the separable potential obtained starting from the straight chain conformer, with an additional constant potential added to it which accounts for the difference between the energies of the global minimum conformer and the straight chain conformer. We have labeled the thermodynamic quantities obtained by using this potential which takes different forms in different regions of phase space as "Piece-sep" (Piecewise separable). Section 3.3.3 discusses how the configurational integral and thermodynamic properties for this potential can be calculated as a sum or product of many different one-dimensional integrals instead of a single multi-dimensional integral.

Using the Piece-sep potential energy we calculate the sum of states and this sum of states does show the desired characteristic of the presence of inflection point which gives rise to the high heat capacity values that we see in Table 3 and Figure 5. There is still the discrepancy between the absolute sum of states of energy between Insep and Piece-sep. The density of states of Insep at low energies is lower because of the assumption of linearity of the potentials between any two grid points which distorts the potential near the energy minimum. The Piece-sep potential on the other hand gives the correct behavior about the energy minimum of a smooth parabolic curve. Based on this reasoning we conclude that the sum of states near low energies, which mainly arise due to the low energy conformer, is more accurate in the case of Piece-sep than in the case of Insep. Also we see that the inflection point is observed at a higher energy in Insep than in Piece-Sep. This is because in Insep the potential at each grid point is calculated without optimizing the geometries which is unlike the Piece-sep in which the relaxed potential scans are used. The single point potentials tend to give higher difference between the lowest energy conformer and other energy minima and thus increases the energy at which the inflection point is seen. We have plotted the heat capacity contribution of the four rotors as a function of temperature for the different cases in Figure 5 to show the improvement in the heat capacity predicted by the Piece-sep over Open-sep and Ring-sep. Also from Table 3 we see a good agreement between Piece-sep and Insep for entropy and enthalpy contributions. Using the efficient numerical method outlined in Section 3.3.3, this method scales much better than the brute force Insep calculations. In the rest of the paper we use the Piece-sep approach to calculate the thermal properties of the hindered rotors.

A further complication arises when the size of the OOQOOH molecule increases. As we have said before, for all OOQOOH molecules the ring conformer which leads to the stabilizing hydrogen bond is the lowest energy conformer. The number of different ring conformers that contain hydrogen bonds increases as the size of the ring increases. Based on the conformational analysis we have performed to get the lowest energy conformer (see Section 2) we find that $HOOCH_2CH_2OO$ has 1 low energy ring conformer, $HOOCH_2CH_2CH_2OO$ has two low energy ring conformers of almost exactly the same energy but in addition to these two there are other straight chain conformers that are very close in energy to the lowest energy conformer, $HOO(CH_2)_4OO$ has multiple ring conformers but the stablest one is more than 2 kcal/mole lower in energy than the rest of the conformers and $HOO(CH_2)_5OO$ has many different ring shaped conformers but six of these are more stable than the rest of the conformers.

Based on these observations we propose the following schemes for calculating the thermodynamic contribution of the hindered rotors. For all OOQOOH molecules we have identified upto six low lying conformers and have calculated the potential using the procedure outlined earlier called Piece-sep. The regions $\mathcal{A}$ corresponding to the hypercube around these low energy conformers, with the rotor dihedral angles taking values $\pm 60^o$ around the equilibrium values. The calculations are expected to get more accurate as the number of conformers on which potential scans are performed is increased. To keep the number of quantum calculations to a reasonable number we have chosen the six or less lowest energy conformers. Note that all the methyl rotors of OOQOOH are treated separately from the rest of the rotors because their potential, to a very good approximation, is independent of the other rotors. The geometries of the low energy conformers for all OOQOOH molecules is given in the supporting information.

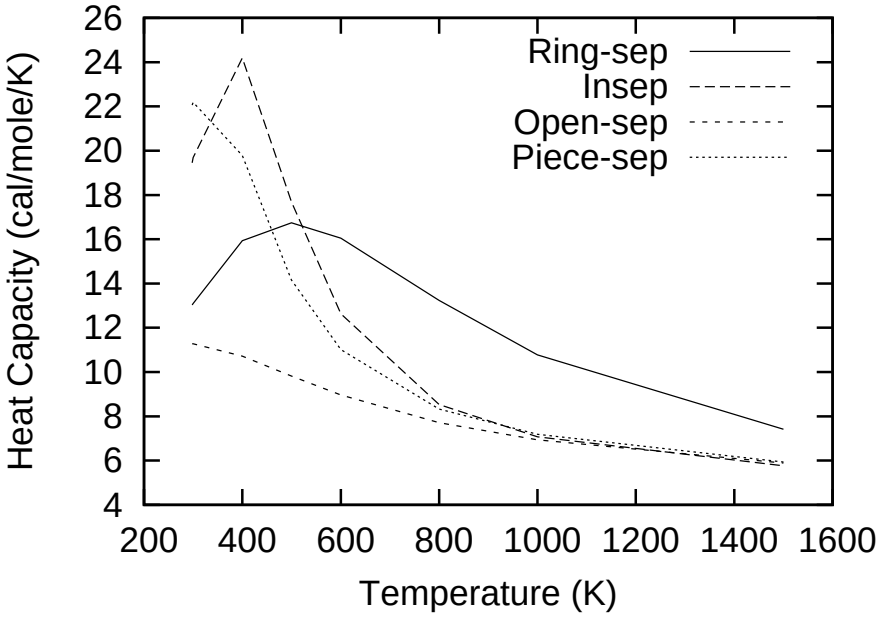

Figure 5: The heat capacity contribution of the four rotors in $HOOCH_2CH(CH_3)OO$ (all except the methyl rotors) calculated using various methods. The meanings of the labels is described in the caption of Figure 4.

3.3.3 Efficient evaluation of the multi-dimensional integral and thermochemistry

For the Piece-sep method, we can significantly simplify the calculation of a n-dimensional configurational integral for n rotors into a product of one-dimensional integrals. For this we divide the configurational space into different parts labeled $\mathcal{A}$ and $\mathcal{B}$ as defined in the previous section. The configuration integral can then be simplified as shown below in Equation 8.

$$
\begin{aligned}
CI &= \int_{\mathcal{A}+\mathcal{B}} \exp(-V(\phi_1,\phi_2,..\phi_n)/k_bT)d\phi_1 d\phi_2..d\phi_n \\
&= \int_{\mathcal{A}} \exp(-V_R(\phi_1,\phi_2,..\phi_n)/k_bT)d\phi_1 d\phi_2..d\phi_n + \int_{\mathcal{B}} \exp(-V_S(\phi_1,\phi_2,..\phi_n)/k_bT)d\phi_1 d\phi_2..d\phi_n \\
&= \int_{\mathcal{A}} \exp(-V_R(\phi_1,\phi_2,..\phi_n)/k_bT)d\phi_1 d\phi_2..d\phi_n + \int_{\mathcal{B}+\mathcal{A}} \exp(-V_S(\phi_1,\phi_2,..\phi_n)/k_bT)d\phi_1 d\phi_2..d\phi_n \\
&\quad - \int_{\mathcal{A}} \exp(-V_S(\phi_1,\phi_2,..\phi_n)/k_bT)d\phi_1 d\phi_2..d\phi_n \\
&= \prod_{i=1}^{n} \int_{\phi_i=-60^o}^{60^o} \exp(-V_{i,R}(\phi_i)/k_bT)d\phi_i + \prod_{i=1}^{n} \int_{\phi_i=-180^o}^{180^o} \exp(-V_{i,S}(\phi_i)/k_bT)d\phi_i \\
&\quad - \prod_{i=1}^{n} \int_{\phi_i=-60^o}^{60^o} \exp(-V_{i,S}(\phi_i)/k_bT)d\phi_i
\end{aligned} \tag{8}
$$

In the above equation V_S is the potential of Equation 1 calculated using the hindered rotors scans starting from the straight chain conformer and V_R is the potential of Equation 1 calculated using the hindered rotors scans starting from the ring conformer. The above formula is fairly easy to code but the expressions for entropy, thermal correction and heat capacity turn out to be quite complicated. To generate the code for the calculation of these thermodynamic quantities conveniently and without errors we use the Automatic Differentiation code Tapenade.[60] All the thermodynamic quantities are generated by calculating the first or the second derivative of the natural log of the partition function. The Fortran codes to calculate the first and second derivatives are calculated using Tapenade. The formulas for multiple $\mathcal{A}$ regions are easily obtained by the extension of Equation 8.

3.4 Thermochemistry

The thermochemical properties of all the reactants and products for the reactions studied here are listed in Table 5. Figure 6 shows the heat of formation given in Table 5 plotted against the difference between the heat of formation computed using Benson's group additivity method and the CBS-QB3 value. The Benson's group additivity used here is the one implemented in Reaction Mechanism Generator (RMG).[61,62] The graph on Figure 6 shows a cluster of positive deviations for ROO radicals and OOQOOH radicals but not for QOOH radicals suggesting a more careful look at D(ROO–H) bond values might lead to resolution of this discrepancy.

The D(ROO–H) in RMG comes from Lay et al.[63] Lay et al. have used isodesmic reactions and MP4SDTQ/6-31G*//MP2/6-31G* and G2 ab initio calculations to calculate heats of formation and subsequently the ROO–H bond dissociation energies for R = methyl, ethyl, iso-propyl, and t-butyl. The group values by Simmie et al.[64] were derived by using heats of formation of a series of ROO species calculated using CBS-QB3 and highly accurate CBS-APNO levels of theory via isodesmic and atomization procedures. Based on the higher level ab initio theory used by Simmie et al. we recommend using their new bond dissociation energy values D(ROO–H) for R = methyl, ethyl, n-propyl,

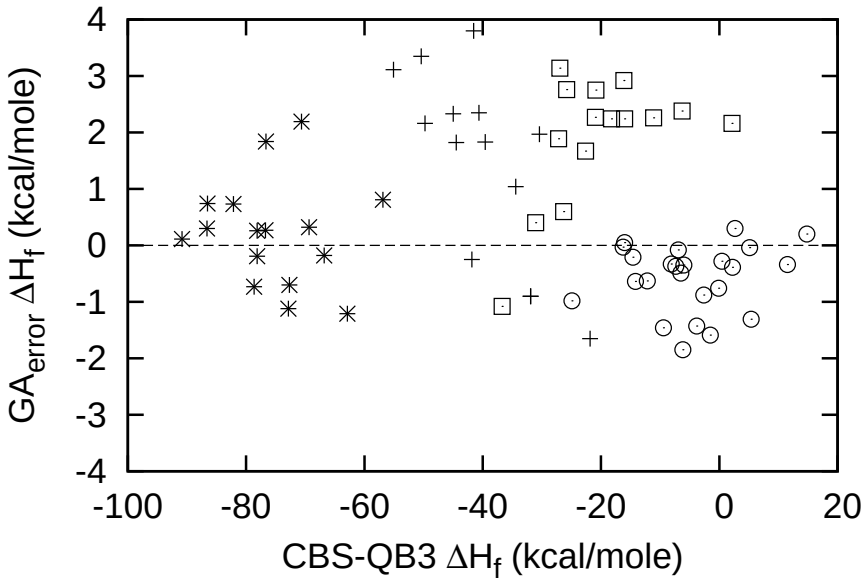

Figure 6: Difference between the heat of formation calculated using Benson's group additivity method and the CBS-QB3 method on the y-axis vs the heat of formation calculated using CBS-QB3 method. + corresponds to OOQOOH molecules; ∗ corresponds to ketohydroperoxide molecules; □ corresponds to ROO; ∘ corresponds to QOOH

i-propyl, n-butyl, t-butyl, i-butyl and s-butyl. In addition to using Simmie et al.'s ROO–H bond dissociation values we also recommend the enthalpy values for extended groups $C(H)_2(OO)(C(OO))$ and $C(H)(OO)(C)(C(OO))$, shown in Figure 7 as -6.6 kcal/mole and -5.7 kcal/mole respectively.

The group value of each of the new groups is derived by respectively adding 1.5 kcal/mole to the group values of $C(H)_2(O)(C)$ and $C(H)(O)(C)_2$ recommended in Benson's book.[65] These new recommended group values are required to accurately predict the heats of formations of all the reactants undergoing 1,4-hydrogen shift in Table 7. The group additivity values for ROO and OOQOOH were recalculated using the Simmie et al. values and the two new group values introduced in this paper and the deviations are again plotted in Figure 8. Here we see that the scatter of the errors is more evenly distributed about the 0 kcal/mole line.

To test the accuracy of the corrected group values, we perform the χ^2 statistical test where we assume that probability of obtaining a value of enthalpy x_i for a molecule i is given by a normal distribution whose average is given by the CBS-QB3 value and whose standard deviation is equal to 1 kcal/mole. The value of 1 kcal/mole is slightly higher than the 0.88 kcal/mole rms error calculated for the atomization energy on the G2/97 text set. With this assumption the probability that the group additivity values give the values of heats of formation as inaccurate as given above is given by the p-value in Table 3.4. Traditionally we reject the null hypothesis if the p-value is smaller than 0.05. From the table it is apparent that with the χ^2 test we cannot reject the null hypothesis for any sets of species, implying that group additivity scheme performs adequately for

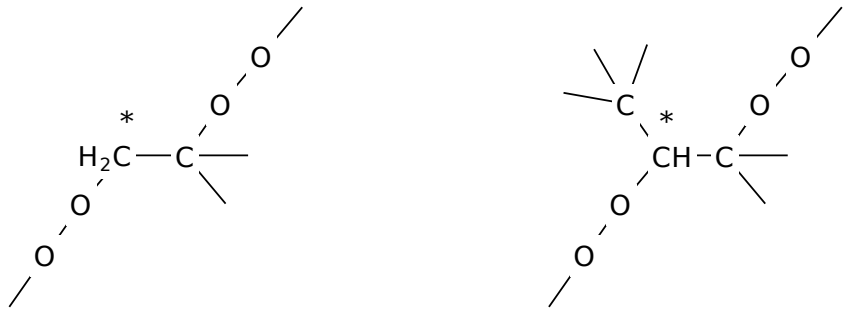

(a) $C(H)_2(OO)(C(OO))$ (b) C(H)(OO)(C)(C(OO))

Figure 7: The extended groups for which new group values are recommended

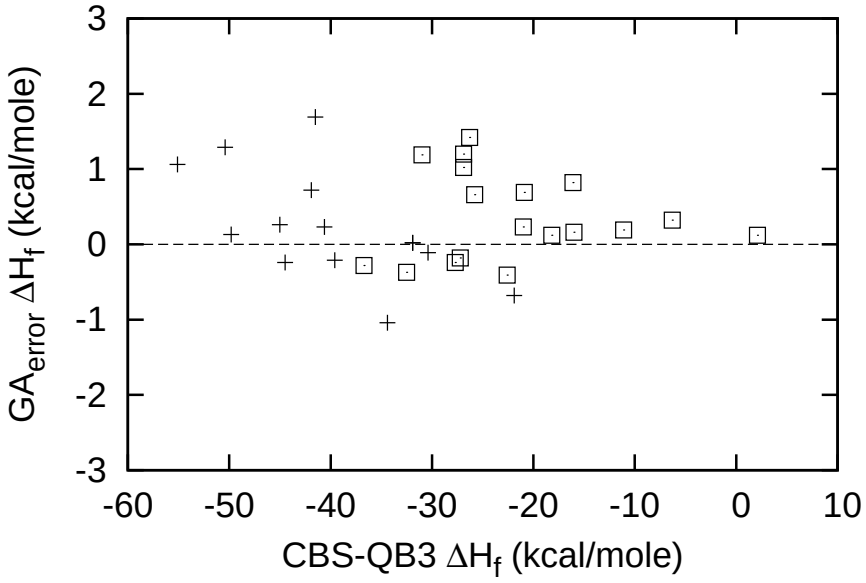

Figure 8: Difference between the heat of formation calculated using Benson's group additivity method with the new updated group values (see text) and the CBS-QB3 method on the y-axis vs the heat of formation calculated using CBS-QB3 method. + corresponds to OOQOOH molecules; □ corresponds to ROO

Molecules	MAD kcal/mole	RMS kcal/mole	χ^2	p-value
ROO	0.53	0.68	7.50	0.98
QOOH	0.62	0.82	16.10	0.85
OOQOOH	0.55	0.76	7.98	0.84
keto	0.69	0.87	10.62	0.64

Table 4: Statistical χ^2 test for the goodness of fit of the group additivity method, where the D(ROO–H) values recommended by Simmie et al. and two new group values introduced in this work were used.

these molecules.

Table 5: Thermochemical values calculated using CBS-QB3 level of theory. H_{298} has units of kcal/mole, S_{298} has units of cal/mole-K and C_p has units of cal/mole-K. [a] These molecules are unstable or metastable.

Molecule	H_{298}	S_{298}	C_p						
			300	400	500	600	800	1000	1500
$HOOCH_2CH_2OO$	-22	89	41	37	38	39	43	46	51
$HOOCH_2CHO$	-57	77	24	28	31	33	37	39	42
$HOOCH_2CH(CH_3)OO$	-32	96	40	42	46	50	55	59	66
$HOOCH(CH_3)CHO$	-67	83	30	35	40	43	48	52	57
$HOOCH(CH_3)CH_2OO$	-32	97	42	41	45	48	54	59	65
$HOOCH_2C(CH_3)O$	-71	84	28	34	39	43	48	52	57
$HOOCH(CH_3)CH(CH_3)OO$	-42	106	40	48	54	60	67	72	80
$HOOCH(CH_3)C(CH_3)O$	-79	93	35	42	48	53	60	64	71
$HOOCH_2CH_2CH_2OO$	-30	103	31	37	42	46	53	57	64
$HOOCH_2CH_2CHO$	-63	90	29	33	36	40	45	49	55
$HOOCH_2CH_2CH(CH_3)OO$	-42	108	39	46	52	57	65	70	79
$HOOCH(CH_3)CH_2CHO$	-73	95	35	41	47	51	58	62	70
$HOOCH(CH_3)CH_2CH_2OO$	-40	110	37	44	51	56	64	70	79
$HOOCH_2CH_2C(CH_3)O$	-77	95	35	42	47	51	58	62	70
$HOOCH(CH_3)CH_2CH(CH_3)OO$	-50	114	44	53	61	67	76	83	93
$HOOCH(CH_3)CH_2C(CH_3)O$	-87	99	41	50	57	62	70	76	85
$HOOCH_2C(CH_3)_2CH_2OO$	-45	113	43	52	60	67	76	83	94
$HOOCH_2C(CH_3)_2CHO$	-78	100	42	50	56	62	70	75	84
$HOO(CH_2)_4OO$	-34	115	38	45	51	57	65	71	80
$HOO(CH_2)_3CHO$	-69	96	35	41	46	51	57	62	70
$HOO(CH_2)_3CH(CH_3)OO$	-45	120	45	53	61	67	77	84	94
$HOOCH(CH_3)(CH_2)_2CHO$	-78	102	42	49	56	61	69	75	85
$HOOCH(CH_3)(CH_2)_3OO$	-44	120	45	53	61	67	77	84	94
$HOO(CH_3)_3C(CH_3)O$	-82	105	40	47	54	60	68	75	84
$HOOCH(CH_3)(CH_2)_2CH(CH_3)OO$	-55	124	52	62	71	78	89	97	109
$HOOCH(CH_3)(CH_2)_2C(CH_3)O$	-91	111	46	56	64	70	80	88	99
$HOO(CH_2)_5OO$	-41	124	44	52	59	66	75	82	93
$HOO(CH_2)_4CHO$	-73	107	40	47	53	59	68	74	84
$HOOCH(CH_3)(CH_2)_4OO$	-50	127	51	61	69	77	87	95	108
$HOO(CH_2)_4C(CH_3)O$	-87	116	45	54	62	68	79	87	98
CH_3OO	2	64	12	14	16	18	21	23	26
CH_3CH_2OO	-6	74	18	21	25	27	32	35	40
$CH_3CH_2CH_2OO$	-11	83	23	29	33	37	43	48	55
$(CH_3)_2CHOO$	-16	81	24	29	34	38	43	48	55
$CH_3CH_2CH_2CH_2OO$	-16	92	29	35	41	46	54	60	69
$(CH_3)_2CHCH_2OO$	-18	89	29	36	42	47	55	60	69
$CH_3CH_2CH(CH_3)OO$	-21	90	30	36	42	47	54	60	69
$(CH_3)_3COO$	-26	86	31	37	42	47	54	60	69
$CH_3CH_2CH_2CH_2CH_2OO$	-21	101	35	43	50	56	65	72	83

Continued on next page

Table 5: Continued from previous page

Molecule	H_{298}	S_{298}	C_p 300	400	500	600	800	1000	1500
$(CH_3)_2CHCH_2CH_2OO$	-23	99	35	43	50	56	65	72	83
$(CH_3)_3CCH_2OO$	-27	93	35	43	51	57	66	73	84
$CH_3CH_2CH_2CH(CH_3)OO$	-26	97	38	45	52	58	67	74	84
$(CH_3)_2CHCH(CH_3)OO$	-27	96	37	44	51	57	66	73	83
$CH_3CH_2C(CH_3)_2OO$	-31	96	37	44	51	57	66	73	83
$CH_3CH_2CH_2CH_2CH_2CH_2OO$	-27	110	42	50	58	65	77	85	98
$(CH_3)_2CHCH_2CH_2CH_2OO$	-28	109	40	49	58	65	76	85	97
$(CH_3)_2CH(CH_2)_4OO$	-33	117	47	57	67	75	88	97	112
$(CH_3)_2CHC(CH_3)_2OO$	-37	102	44	53	60	67	77	85	98
$^aCH_2OOH$	15	67	15	17	19	20	23	24	27
$^aCH_3CH(.)OOH$	5	76	20	23	26	29	33	36	41
$^aCH_3CH_2CH(.)OOH$	0	86	25	30	34	38	44	48	55
$^a(CH_3)_2CHCH(.)OOH$	-7	93	31	38	44	48	56	61	69
$^a(CH_3)_3CCH(.)OOH$	-15	97	37	46	53	58	67	74	84
$HOOCH_2CH_2(.)$	11	79	20	24	27	29	33	36	40
$HOOCH(CH_3)CH_2(.)$	2	85	27	32	36	39	44	48	54
$HOOC(CH_3)_2CH_2(.)$	-7	91	34	40	45	49	56	61	69
$CH_3CH(.)CH_2OOH$	3	90	24	29	33	37	43	47	54
$CH_3CH(.)CH(CH_3)OOH$	-6	96	31	37	43	47	55	60	68
$CH_3CH(.)C(CH_3)_2OOH$	-16	102	38	45	52	58	66	73	83
$(CH_3)_2C(.)CH_2OOH$	-7	97	29	35	41	46	54	59	68
$(CH_3)_2C(.)CH(CH_3)OOH$	-16	102	35	43	50	56	65	72	83
$(CH_3)_2C(.)C(CH_3)_2OOH$	-25	107	42	51	60	67	77	85	97
$HOOCH_2CH_2CH_2(.)$	5	88	25	30	34	38	44	48	54
$HOOCH_2CH(CH_3)CH_2(.)$	-2	94	32	38	44	48	55	61	69
$HOOCH_2C(CH_3)_2CH_2(.)$	-9	100	37	45	53	58	67	74	83
$HOOCH(CH_3)CH_2CH_2(.)$	-4	94	32	38	44	49	56	61	69
$HOOCH(CH_3)_2CH_2CH_2(.)$	-14	100	38	46	53	59	67	74	83
$CH_3CH(.)(CH_2)_2OOH$	-3	98	29	36	42	46	54	60	68
$CH_3CH(.)CH_2CH(CH_3)OOH$	-12	104	36	44	51	57	66	73	83
$HOOCH_2CH_2CH_2CH_2(.)$	0	97	30	37	42	47	55	60	69
$CH_3CH(.)(CH_2)_3OOH$	-8	107	34	42	50	56	65	72	83
$(CH_3)_2C(.)(CH_2)_2OOH$	-11	105	35	43	50	56	65	72	83
$(CH_3)_2C(.)(CH_2)_3OOH$	-17	115	39	48	57	64	75	84	97

3.4.1 Estimated accuracy of thermochemistry

Prior works have demonstrated that at the CBS-QB3 level ΔH_f^{298} is typically accurate to within about 2 kcal/mole, while S^{298} and Cp are usually accurate to within about 1 cal/mole-K. In the present set of molecules we expect larger uncertainties. The wide discrepancies in results obtained using different methods to compute the hindered rotors suggests both S^{298} and Cp could be uncertain by 3 cal/mol-K. From Simmie's analysis of ROO thermochemistry, a conservative estimate of the accuracy of the CBS-QB3 ΔH_f^{298}

reported here are 2 kcal/mole.

3.5 Rate Coefficients

The rates of reactions of many intramolecular-H-migrations of ROO and the intramolecular-H-migration of the H on the C α to the OOH group of OOQOOH, computed at the CBS-QB3 level are given in Table 6 and Table 7 respectively. Some structural features of these rate coefficients are discussed below.

Reactant	k_∞		
	A	n	E_a
1,3-hydrogen shift			
(1,3p)			
CH_3OO	1.1×10^{13}	1.5	42.3
(1,3s)			
CH_3CH_2OO	4.6×10^{12}	1.3	39.7
$CH_3CH_2CH_2OO$	7.9×10^{12}	1.2	39.7
$(CH_3)_2CHCH_2OO$	9.3×10^{12}	1.0	39.6
$(CH_3)_3CCH_2OO$	8.7×10^{12}	1.0	39.3
(1,3t)			
$(CH_3)_2CHOO$	5.3×10^{12}	1.0	38.5
1,4-hydrogen shift			
(1,4p)			
CH_3CH_2OO	5.6×10^{11}	0.2	34.2
$(CH_3)_2CHOO$	9.7×10^{11}	1.1	33.5
$(CH_3)_3COO$	2.0×10^{12}	1.2	33.5
(1,4s)			
$CH_3CH_2CH_2OO$	4.0×10^{11}	1.1	30.1
$CH_3CH_2CH(CH_3)OO$	4.3×10^{11}	0.9	29.5
$CH_3CH_2C(CH_3)_2OO$	4.1×10^{11}	0.7	30.1
(1,4t)			
$(CH_3)_2CHCH_2OO$	5.8×10^{11}	0.8	27.1
$(CH_3)_2CHCH(CH_3)OO$	4.7×10^{11}	0.6	27.3
$(CH_3)_2CHC(CH_3)_2OO$	5.5×10^{11}	0.4	26.4
1,5-hydrogen shift			
(1,5p)			
$CH_3CH_2CH_2OO$	7.5×10^{10}	1.6	21.0
$CH_3CH_2CH(CH_3)OO$	7.6×10^{10}	1.4	20.8
$CH_3CH_2C(CH_3)_2OO$	1.0×10^{11}	1.1	21.9
$(CH_3)_2CHCH_2OO$	1.3×10^{11}	1.3	21.5
$(CH_3)_3CCH_2OO$	5.3×10^{11}	1.2	21.6
(1,5s)			
$CH_3CH_2CH_2CH_2OO$	5.4×10^{10}	1.3	18.2
$CH_3CH_2CH_2CH(CH_3)OO$	1.4×10^{11}	0.2	18.5

Continued on next page

Table 6: Continued from previous page

Reactant	k_∞		
	A	n	E_a
(1,5t)			
$(CH_3)_2CHCH_2CH_2OO$	4.9×10^{10}	1.2	15.4
1,6-hydrogen shift			
(1,6p)			
$CH_3CH_2CH_2CH_2OO$	1.3×10^{10}	1.5	20.0
(1,6s)			
$CH_3CH_2CH_2CH_2CH_2OO$	7.4×10^{9}	1.2	16.6
(1,6t)			
$(CH_3)_2CHCH_2CH_2CH_2OO$	6.8×10^{9}	1.2	13.8
1,7-hydrogen shift			
(1,7p)			
$CH_3(CH_2)_4OO$	3.1×10^{9}	1.5	19.9
(1,7s)			
$CH_3CH_2(CH_2)_4OO$	1.3×10^{9}	1.0	18.2
(1,7t)			
$(CH_3)_2CH(CH_2)_4OO$	1.1×10^{9}	1.1	14.3

Table 6: Computed high-pressure-limit rate coefficients for intramolecular-H-migration of ROO radicals given in the form $k = A\left(\frac{T}{1000}\right)^n \exp(-E_a/RT)$. The unimolecular rate coefficients are in s^{-1}. The units of E_a are kcal/mole. p, s and t indicates whether the H atoms being abstracted are primary, secondary or tertiary.

3.5.1 Effect of transition state ring size

The size of ring is the most important determinant for the rate of reaction of intramolecular-H-migration reactions. In general one would expect that increasing the size of ring of the transition state will release some of the ring strain and reduce the activation energy of the reactions. But at the same time as the ring size increases it tends to tie up more hindered rotors and thus reduces the entropy of the transition state. Thus the increase in the ring size decreases the pre-exponential factor and also decreases the activation energy of the reactions. This effect is indeed observed in our data, with activation energy decreasing sharply from 4 membered ring transition state to 8 membered ring transition states and pre-exponential factor also decreasing with the increase in the ring size.

3.5.2 Effect of methyl groups α to the hydrogen losing carbon atom

One might expect the A factor for the abstraction of primary(p) > secondar(s) > tertiary(t) due to the different number of hydrogen atoms. From Table 6 one can also observe that for intramolecular-H-migration in ROO the activation energy depends quite strongly on how many methyl groups are present on the carbon atom that is losing the hydrogen

Reactant	k_∞		
	A	n	E_a
1,4-hydrogen shift			
$HOOCH_2CH_2OO$	8.0×10^{9}	4.2	25.8
$HOOCH_2CH(CH_3)OO$	4.4×10^{10}	2.5	28.7
$HOOCH(CH_3)CH_2OO$	3.3×10^{10}	2.7	26.3
$HOOCH(CH_3)CH(CH_3)OO$	3.5×10^{10}	0.6	27.6
1,5-hydrogen shift			
$HOOCH_2CH_2CH_2OO$	1.8×10^{10}	2.8	18.8
$HOOCH_2CH_2CH(CH_3)OO$	1.7×10^{10}	2.9	18.1
$HOOCH_2C(CH_3)_2CH_2OO$	4.0×10^{10}	2.4	18.8
$HOOCH(CH_3)CH_2CH_2OO$	1.7×10^{10}	2.4	17.8
$HOOCH(CH_3)CH_2CH(CH_3)OO$	3.1×10^{10}	2.1	17.5
1,6-hydrogen shift			
$HOO(CH_2)_4OO$	2.9×10^{8}	3.0	19.7
$HOO(CH_2)_3CH(CH_3)OO$	3.2×10^{8}	3.0	19.8
$HOOCH(CH_3)(CH_2)_3OO$	3.2×10^{8}	2.5	16.9
$HOOCH(CH_3)(CH_2)_2CH(CH_3)OO$	4.6×10^{8}	2.4	17.1
1,7-hydrogen shift			
$HOO(CH_2)_5OO$	9.3×10^{7}	3.8	17.1
$HOOCH(CH_3)(CH_2)_4OO$	8.0×10^{7}	3.3	14.7

Table 7: Computed high-pressure-limit rate coefficients for intramolecular-H-migration OOQOOH $\rightarrow$ HOOQO + OH in the form $k = A\left(\frac{T}{1000}\right)^n \exp(-E_a/RT)$. The unimolecular rate coefficients are in s^{-1}. The units of E_a are kcal/mole.

atom. For example for 1,4-hydrogen migration, presence of the one methyl group on the carbon atom losing hydrogen causes the activation energy of the reaction to decrease by 4.1 kcal/mole and the presence of the second methyl group causes a further drop in the activation energy by 3 kcal/mole. Similar 3-4 kcal/mole decreases in the activation energy due to the presence of the methyl group are observed for other transition states in this family. The presence of the methyl group is expected to decrease the strength of the C–H bond which is being broken and hence is expected to cause a decrease in the activation energy. Besides the weakening of C–H bond the methyl group can have other complicated steric effects for reactions of OOQOOH because both the reactant and transition state are ring shaped. Table7 shows that the presence of a methyl radical on the hydrogen losing carbon atom in OOQOOH, with a few exceptions, also has the effect of reducing the activation energy by about 1-2 kcal/mole.

3.5.3 Performance of B3LYP method

In Section 3.2 we have seen that B3LYP/CBSB7 method gives very good agreement with CBS-QB3 method for intramolecular-H-migration in OOQOOH but over-predicts the barrier height for ROO. In Figure 9 also we see that the best fit line for ROO suggests that B3LYP/CBSB7 method over-predicts the barrier height compared to CBS-QB3 method but on an average gives equal barrier height as CBS-QB3 method for OOQOOH. This seems to suggest that B3LYP/CBSB7 method is quite accurate for OOQOOH → HOOQO + OH, probably due to fortuitous cancellation of errors.

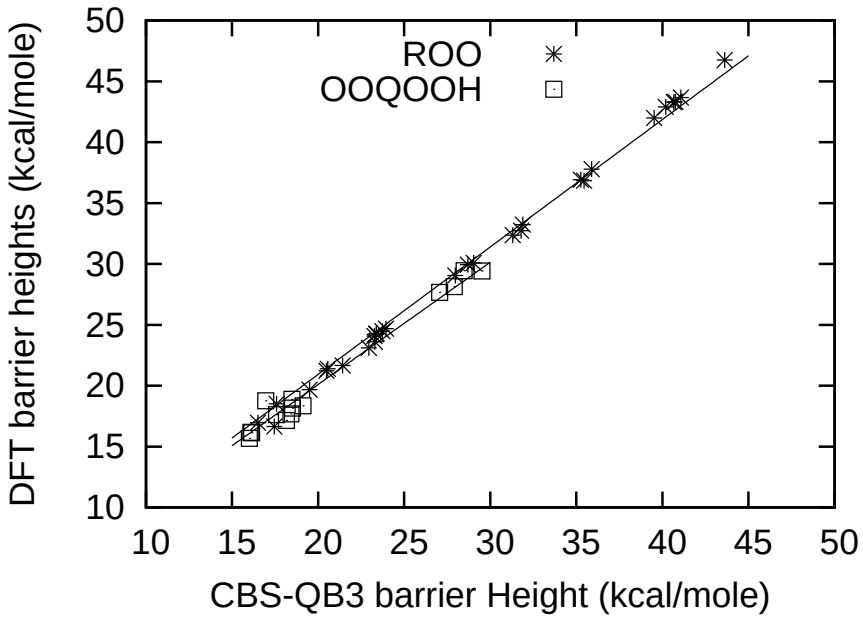

Figure 9: Barrier heights calculated using B3LYP/CBSB7 (labeled DFT) vs barrier heights calculated using CBS-QB3 method. For OOQOOH $y = x$ is the best fit line and for ROO $y = 1.05x$ the best fit line.

3.5.4 Comparison with literature data

We here compare our calculated activation energies and barrier heights with those published previously in the literature.

The ZPE corrected barrier height calculated for 1,5-hydrogen migration in $CH_3C(CH_3)_2CH_2OO$ by Sun et al[33] is 23.8 kcal/mole which is in good agreement with the barrier height calculated in our study of 23.4 kcal/mole. Hughes et al. have indirectly measured the rate of the same reaction at 700 K as 1.2×10^3 s^{-1} where as we get a value of 6.2×10^4 s^{-1}, Sun et al. obtain a value of 3.9×10^4 s^{-1}, and Baldwin et al.[66] give a rate constant of 1.3×10^4 s^{-1}. In a recent paper by Petway et al.[23] the OH yield was spectroscopically measured and the PES computed by Sun et al. was found to be adequate in explaining the experimental measurements. Curran et al.[36] estimated a rate coefficient of $2.2 \times 10^{12} \exp(-23.9 \text{ kcal}/RT)$ which for 700 K gives a value of 7.8×10^4 s^{-1}.

1,5-hydrogen migration barrier height has also been calculated in ROO where R = n-propyl by DeSain et al[20] as 23.7 kcal/mole using their composite "HL2" method which is in very good agreement with our CBS-QB3 value of 23.4 kcal/mole.

The 1,4-hydrogen migration barrier heights have been calculated for ethylperoxyl by Sheng et al.[25] as 36.3 kcal/mole, by Carstensen et al[3] as 35.9 kcal/mole, and by Miller et al[26] as 36.0 kcal/mol, which all agree very well with the value of 35.9 kcal/mole calculated here (note Carstensen et al. have also used CBS-QB3 method for their calculations and get exactly the same barrier height as us). DeSain et al. have calculated ROO hydrogen migration reaction barrier heights for various R groups which we reproduce here in Table 8 along with values from our present study. The comparison between our barrier heights and other rigorous studies in the literature show good agreement. There are a few cases where the difference between a barrier height calculated by us and taken from literature is 2 kcal/mole which is entirely within the error bars of the methods employed here. As shown by DeSain et al.[13] even with the state of the art quantum chemical methods and rate calculation methods, some fine adjustment of the rate parameters is required to get a good agreement between theory and experiments.

After the formation of QOOH, another O_2 atom can add on to it to form OOQOOH which again undergoes intramolecular-H-migration followed by O–O bond fission. Sun et al.[33] have calculated the Arrhenius parameters of reaction for $HOOCH_2C(CH_3)_2CH_2OO$ as $A = 9.8 \times 10^5$ $s^{-1}K^{-1.1}$, $n = 1.1$ and $E_a = 22.0$ kcal/mole. The Arrhenius parameters calculated in this study for the same reaction are $A = 1.0 \times 10^3$ $1/s/K^{2.4}$, $n = 2.4$ and $E_a = 18.8$ kcal/mole. The two sets of Arrhenius parameters given here are on a per-hydrogen atom basis and the rate coefficients are calculated by the expression $k = AT^n \exp(-E_a/R/T)$. The activation energy of Sun et al. is higher by about 3.0 kcal/mole compared to ours and the reason is that the transition state used by them to calculate the rate coefficient is not the minimum energy conformer. When we use their transition state geometry with the CBS-QB3 method to calculate the rate coefficient we get the same activation energy as they do. This suggests that the barrier height and the rate coefficients calculated by Sun et al. for this particular reaction are inaccurate and need to be revised. The barrier height for 1,4-hydrogen transfer in $HOOCH_2CH_2OO$ radical was calculated to be 29.7 kcal/mole and 31.2 kcal/mole by Bozzelli et al[24] using CBS-Q//B3LYP/6-31G(d,p) and G3(MP2) method respectively both of which compare very well with the value calculated in this study of 30.7 kcal/mole.

R	TS	ΔE (0 K)		
		DeSain	Present	Others
n-C_3H_7	(1,4s)	32.3	31.9	31.7[67]
i-C_3H_7	(1,4p)	35.4	35.3	
n-C_4H_9	(1,4s)	33.4	31.9	
	(1,5s)	22.3	20.6	20.3[68] ,22.7[b 69]
	(1,6p)	23.9	22.9	25.5[68]
sec-C_4H_9	(1,4p)	37.0	35.3[a]	
	(1,4s)	32.8	31.3	
	(1,5p)	24.6	23.3	24.3[68] ,25.4[b 69]
iso-C_4H_9	(1,4t)	29.7	28.7	28.4[32]
	(1,5p)	24.3	23.7	21.0[32]
tert-C_4H_9	(1,4p)	37.9	35.5	32.8[32]

Table 8: Table comparing the ZPE corrected barrier heights for ROO isomerization calculated by DeSain et al[13] and the ones calculated in the present study. [a]is taken from (1,4p) of i-C_3H_7 because we have not calculated the (1,4p) TS in sec-C_4H_9. [b] is taken from barrier heights calculated in alpha peroxy radicals of methyl butanoate and methyl pentanoate.

In papers by Curran for the oxidation of heptane[70] and iso-octane[71] they have assumed that the intramolecular-H-migration of OOQOOH has an A-factor which is 0.5 of and activation energy which is 3 kcal/mole less than the corresponding ROO isomerization reaction. When we compare the activation energies of unbranched ROO and OOQOOH from Table 6 and Table 7, we see that the difference for 1,4-migration is 8.6 kcal/mole, for 1,5-migration is 2.2 kcal/mole, for 1,6-migration is 0 kcal/mole and for 1,7-migration is 2.8 kcal/mole. Also in most of the mechanisms OOQOOH only abstracts a hydrogen atom from the carbon atom directly bonded to the OOH group. Because this C–H bond is weaker than a normal alkane C–H bond, this is often a reasonable approximation. But for the case of say $OOCH_2CH(OOH)CH_3$, the rate of migration of the H atom from the C bonded to OOH group at 700 K is 7.8×10^1 s^{-1} and for migration from the CH_3 group is 3.6×10^4 s^{-1}. As a result significant pathways from OOQOOH are missing from kinetic models, which underscores the importance of rate based automated mechanism generators for exhaustively exploring important pathways.

3.5.5 Evans-Polanyi plots

Figure 10 shows the Evans-Polanyi plots for the intramolecular-H-migration in the ROO radicals. These reactions are all endothermic and so we expect the $dE_a/d\Delta H$ to be greater than 0.5 but less than 1. The slopes of these graphs ≈ 1 for all the ring sizes. We have also plotted the Evans-Polanyi plots for intramolecular-H-migration in OOQOOH radicals in Figure 11. These reactions are highly exothermic but have a slope $dE_a/d\Delta H \approx 0.5$.

To understand these trends let us first consider the intramolecular-H-migration of ROO radicals. The reaction consists of the simultaneous breaking of a C–H bond and formation of an O–H bond and the heat of reaction really depends on the total energy

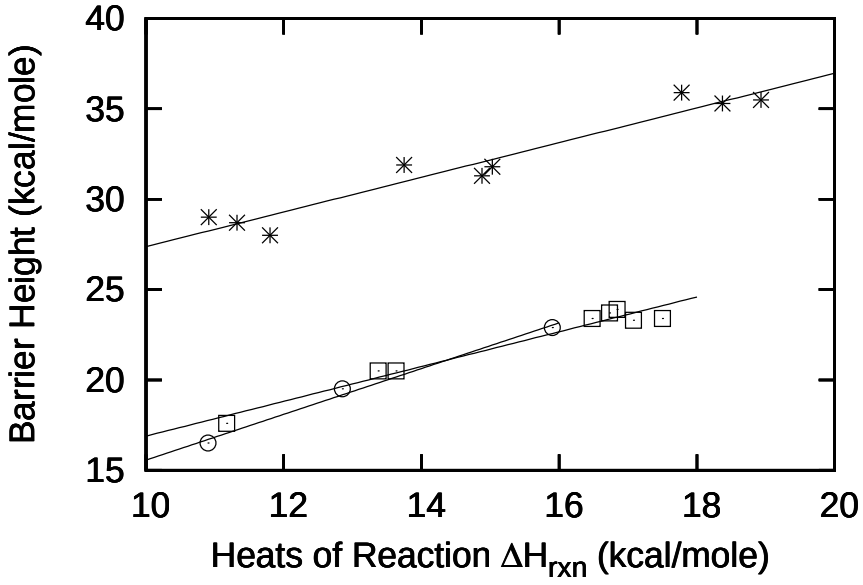

Figure 10: Evans-Polanyi plots for the intramolecular-H-migration of ROO radicals. $*$ corresponds to 1,4-H migration; $\square$ corresponds to 1,5-H migration; $\circ$ corresponds to 1,6-H migration. The fits for (1,4), (1,5) and (1,6) hydrogen migration are $E_a = 0.96\Delta H$+17.78, $E_a = 0.96\Delta H + 7.26$ and $E_a = 1.26\Delta H + 2.91$ respectively.

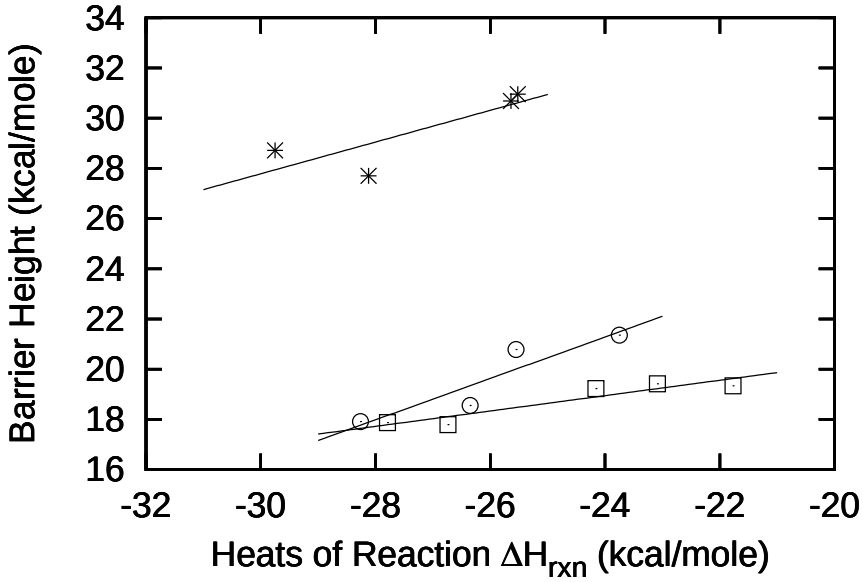

Figure 11: Evans-Polanyi plots for the intramolecular-H-migration of OOQOOH radicals. $*$ corresponds to 1,4-H migration; $\square$ corresponds to 1,5-H migration; $\circ$ corresponds to 1,6-H migration. The fits for (1,4), (1,5) and (1,6) hydrogen migration are $E_a = 0.63\Delta H + 46.74$, $E_a = 0.31\Delta H + 26.29$ and $E_a = 0.82\Delta H + 41.06$ respectively.

gained or lost in the chemical process of bond breaking and bond forming. The slope of 1 seems to suggest that for the forward reaction the C–H bond is almost fully broken and O–H bond is almost fully formed in the transition state. But now if we consider the OOQOOH intramolecular-H-migration, in addition to C–H bond breaking and O–H bond forming, the breaking of the O–OH bond also occurs. The O–OH bond break releases a lot of energy making this reaction exothermic, but this bond breaking happens at a later stage in the reaction and we do not expect it to affect the transition state very much. The other two chemical processes are the same in OOQOOH as in ROO with the only difference now, that the O–H bond is not as well formed in case of OOQOOH as in the case of ROO which can be confirmed by comparing the O–H bond lengths in Table 1 and Table 2. Thus the total effect of O–H bond forming and C–H bond breaking on the heat of formation is split more evenly before and after the transition state and we get a slope closer to 0.5.

4 Conclusions

In this paper we have calculated the thermochemistry and rate coefficients for a series of reactions and molecules involved in the intra-molecular hydrogen transfer in alkylperoxy radicals and hydroperoxyalkylperoxy radicals. Although there are only limited experimental data, CBS-QB3 method seems to be adequate for predicting the energies and barrier heights of the reactions. The treatment of hindered rotors for OOQOOH molecules is complicated by the fact that the shape of one hindered rotor's potential is influenced strongly by the value of the dihedral angle of other hindered rotors. We have suggested that the conformational space of the molecule should be subdivided into low energy parts for which local accurate potential energy surfaces are required and the rest of the region where the potential energy can be predicted by the usual independent hindered rotation approximation for a suitably chosen conformer. Using this method we have demonstrated that the calculated thermochemical contributions of the rotors are in good agreement with those calculated using the full multidimensional configurational integral. This method is used to calculate the thermochemistry and the rate coefficients for the intramolecular-H-migrations of OOQOOH molecules.

The rate coefficients follow the usual trends that we expect to see with the increase in the size of the ring. The thermochemistry of the molecules is predicted well by Benson's group additivity method when the latest group values for bond dissociation of ROO–H from the literature are used and new group values for $C(H)_2(OO)(C(OO))$ and C(H)(OO)(C)(C(OO)) suggested here are used. Finally we have tabulated the rate coefficients and thermochemistry calculated for easy reference and use in large chemical mechanisms.

5 Acknowledgments

This work was funded by the US Department of Energy, Office of Basic Energy Sciences, Division of Chemical Sciences, Geosciences, and Biosciences, under contract DE-FG02-98ER14914. Additional support from NSF Grant CHE-0535604, Collaborative Research in Process Informatics for Chemical Reaction Systems, is also gratefully acknowledged.

6 Supporting Information

Cartesian coordinates of all the optimized structures of all the molecules and transition states are given. This material is available free of charge via the Internet at http://pubs.acs.org.

References

(1) Warnatz, J.; Maas, U.; Dibble, R. W. *Combustion : physical and chemical fundamentals, modeling and simulation, experiments, pollutant formation*; Springer, 2001.

(2) Rienstra-Kiracofe, J. C.; Allen, W. D.; Schaefer, I., Henry F. *J. Phys. Chem. A* **2000**, *104*, 9823–9840.

(3) Carstensen, H.-H.; Naik, C. V.; Dean, A. M. *J. Phys. Chem. A* **2005**, *109*, 2264–2281.

(4) Wijaya, C. D.; Sumathi, R.; Green, W. H. *J. Phys. Chem. A* **2003**, *107*, 4908–4920.

(5) Baldwin, R. R.; Walker, R. W.; Yorke, D. A. *J. Chem. Soc., Faraday Trans. 1* **1973**, *69*, 826–32.

(6) Baker, R. R.; Baldwin, R. R.; Fuller, A. R.; Walker, R. W. *J. Chem. Soc., Faraday Trans. 1* **1975**, *71*, 736–55.

(7) Baker, R. R.; Baldwin, R. R.; Walker, R. W. *J. Chem. Soc., Faraday Trans. 1* **1975**, *71*, 756–79.

(8) Baldwin, R. R.; Cleugh, C. J.; Walker, R. W. *J. Chem. Soc., Faraday Trans. 1* **1976**, *72*, 1715–22.

(9) Atri, G. M.; Baldwin, R. R.; Evans, G. A.; Walker, R. W. *J. Chem. Soc., Faraday Trans. 1* **1978**, *74*, 366–79.

(10) Baldwin, R. R.; Walker, R. W.; Walker, R. W. *J. Chem. Soc., Faraday Trans. 1* **1980**, *76*, 825–37.

(11) DeSain, J. D.; Klippenstein, S. J.; Taatjes, C. A. *Phys. Chem. Chem. Phys.* **2003**, *5*, 1584–1592.

(12) Clifford, E. P.; Farrell, J. T.; DeSain, J. D.; Taatjes, C. A. *J. Phys. Chem. A* **2000**, *104*, 11549–11560.

(13) DeSain, J. D.; Clifford, E. P.; Taatjes, C. A. *J. Phys. Chem. A* **2001**, *105*, 3205–3213.

(14) Taatjes, C. A.; Oh, D. B. *Appl. Opt.* **1997**, *36*, 5817–5821.

(15) Taatjes, C. A. *J. Phys. Chem. A* **2006**, *110*, 4299–4312.

(16) Kaiser, E. W. *J. Phys. Chem.* **1995**, *99*, 707–11.

(17) Kaiser, E. W.; Wallington, T. J. *J. Phys. Chem.* **1996**, *100*, 18770–18774.

(18) Kaiser, E. W. *J. Phys. Chem. A* **1998**, *102*, 5903–5906.

(19) Kaiser, E. W. *J. Phys. Chem. A* **2002**, *106*, 1256–1265.

(20) DeSain, J. D.; Taatjes, C. A.; Miller, J. A.; Klippenstein, S. J.; Hahn, D. K. *Faraday Discuss.* **2001**, *119*, 101–120.

(21) Estupinan, E. G.; Klippenstein, S. J.; Taatjes, C. A. *J. Phys. Chem. B* **2005**, *109*, 8374–8387.

(22) DeSain, J. D.; Klippenstein, S. J.; Miller, J. A.; Taatjes, C. A. *J. Phys. Chem. A* **2003**, *107*, 4415–4427.

(23) Petway, S. V.; Ismail, H.; Green, W. H.; Estupinan, E. G.; Jusinski, L. E.; Taatjes, C. A. *J. Phys. Chem. A* **2007**, *111*, 3891–3900.

(24) Bozzelli, J. W.; Sheng, C. *J. Phys. Chem. A* **2002**, *106*, 1113–1121.

(25) Sheng, C. Y.; Bozzelli, J. W.; Dean, A. M.; Chang, A. Y. *J. Phys. Chem. A* **2002**, *106*, 7276–7293.

(26) Miller, J. A.; Klippenstein, S. J.; Robertson, S. H. *Proc. Combust. Inst.* **2000**, *28*, 1479–1486.

(27) Ignatyev, I. S.; Xie, Y.; Allen, W. D.; Schaefer, I., Henry F. *J. Chem. Phys.* **1997**, *107*, 141–155.

(28) Estupinan, E. G.; Jusinski, L. E.; Klippenstein, S. J.; Taatjes, C. A. Abstracts of Papers, 228th ACS National Meeting, Philadelphia, PA, United States, August 22-26, 2004 PHYS–492, 2004.

(29) Estupinan, E. G.; Smith, J. D.; Tezaki, A.; Klippenstein, S. J.; Taatjes, C. A. *J. Phys. Chem. A* **2007**, *111*, 4015–4030.

(30) Bozzelli, J. W.; Pitz, W. J. *Symp. (Int.) Combust., [Proc.]* **1994**, *25th*, 783–91.

(31) Chen, C.-J.; Bozzelli, J. W. *Chem. Phys. Processes Combust.* **1995**, 381–4.

(32) Chen, C.-J.; Bozzelli, J. W. *J. Phys. Chem. A* **1999**, *103*, 9731–9769.

(33) Sun, H.; Bozzelli, J. W. *J. Phys. Chem. A* **2004**, *108*, 1694–1711.

(34) Sun, H.; Bozzelli, J. W.; Law, C. K. *J. Phys. Chem. A* **2007**, *111*, 4974–4986.

(35) Wang, S.; Miller, D. L.; Cernansky, N. P.; Curran, H. J.; Pitz, W. J.; Westbrook, C. K. *Combust. Flame* **1999**, *118*, 415–430.

(36) Curran, H. J.; Pitz, W. J.; Westbrook, C. K.; Hisham, M. W. M.; Walker, R. W. *Symp. (Int.) Combust., [Proc.]* **1996**, *26th*, 641–649.

(37) Chan, W.-T.; Hamilton, I. P.; Pritchard, H. O. *J. Chem. Soc., Faraday Trans.* **1998**, *94*, 2303–2306.

(38) Pfaendtner, J.; Yu, X.; Broadbelt, L. J. *J. Phys. Chem. A* **2006**, *110*, 10863–10871.

(39) Frisch, M. J. et al. *Gaussian 03, Revision C.02*, Gaussian, Inc., Wallingford, CT, 2004.

(40) Montgomery, J. A.; Ochterski, J. W.; Petersson, G. A. *Journal of Chemical Physics* **1994**, *101*, 5900–5909.

(41) Ochterski, J. W.; Petersson, G. A.; Montgomery, J. A. *Journal of Chemical Physics* **1996**, *104*, 2598–2619.

(42) Montgomery, J. A.; Frisch, M. J.; Ochterski, J. W.; Petersson, G. A. *Journal of Chemical Physics* **2000**, *112*, 6532–6542.

(43) Curtiss, L. A.; Raghavachari, K.; Trucks, G. W.; Pople, J. A. *Journal of Chemical Physics* **1991**, *94*, 7221–7230.

(44) East, A. L. L.; Radom, L. *Journal of Chemical Physics* **1997**, *106*, 6655–6674.

(45) Vansteenkiste, P.; Speybroeck, V. V.; Pauwels, E.; Waroquier, M. *Chemical Physics* **2005**, *314*, 109–117.

(46) Speybroeck, V. V.; Vansteenkiste, P.; Neck, D. V.; Waroquier, M. *Chemical Physics Letters* **2005**, *402*, 479–484.

(47) Wilson, B. E. J.; Decius, J. C.; Cross, P. C. *Molecular Vibration. The Theory of Infrared and Raman Vibrational Spectra.*; Dover Publications, Inc. New York, 1980.

(48) Miller, W. H.; Handy, N. D.; Adams, J. E. *Journal of chemical physics* **1980**, *72*, 99–112.

(49) Vansteenkiste, P.; Van Neck, D.; Van Speybroeck, V.; Waroquier, M. *J Chem Phys 124*, 044314.

(50) Scott, A. P.; Radom, L. *Journal of Physical Chemistry* **1996**, *100*, 16502–16513.

(51) Petersson, G. A.; Malick, D. K.; Wilson, W. G.; Ochterski, J. W.; Montgomery, J. A.; Frisch, M. J. *Journal of Chemical Physics* **1998**, *109*, 10570–10579.

(52) Hirschfelder, J. O.; Wigner, E. *Journal of Chemical Physics* **1939**, *7*, 616–628.

(53) Mill, T.; Montorsi, G. *Int. J. Chem. Kinet.* **1973**, *5*, 119–36.

(54) Mill, T.; Hendry, D. G. Compr. Chem. Kinet. 1–87, 1980.

(55) Vana Sickle, D. E.; Mill, T.; Mayo, F. R.; Richardson, H.; Gould, C. W. *J. Org. Chem.* **1973**, *38*, 4435.

(56) Malick, D. K.; Petersson, G. A.; Montgomery, J. A. *Journal of Chemical Physics* **1998**, *108*, 5704–5713.

(57) Asatryan, R.; Bozzelli, J. W. *Chem. Phys. Processes Combust.* **2007**, a17/1–a17/6.

(58) Welz, O.; Striebel, F.; Olzmann, M. *Phys. Chem. Chem. Phys.* **2008**, *10*, 320–329.

(59) Edinoff, M. L.; Aston, J. G. *Journal of Chemical Physics* **1935**, *3*, 379–383.

(60) Hascoet, L.; Pascual, V. *TAPENADE 2.1 user's guide*.

(61) Song, J. Ph.D. thesis, Massachusetts Institute of Technology, 2004.

(62) Yu, J. Ph.D. thesis, Massachusetts Institute of Technology, 2004.

(63) Lay, T. H.; Bozzelli, J. W. *J. Phys. Chem. A* **1997**, *101*, 9505–9510.

(64) Simmie, J. M.; Black, G.; Curran, H. J.; Hinde, J. P. *J. Phys. Chem. A* **2008**, *112*, 5010–5016.

(65) Benson, S. W. *Thermochemical Kinetics, Methods for the Estimation of Thermochemical Data and Rate Parameters*; John Wiley & Sons, 1976.

(66) Baldwin, R. R.; Hisham, M. W. M.; Walker, R. W. *J. Chem. Soc., Faraday Trans. 1* **1982**, *78*, 1615–27.

(67) Merle, J. K.; Hayes, C. J.; Zalyubovsky, S. J.; Glover, B. G.; Miller, T. A.; Hadad, C. M. *J. Phys. Chem. A* **2005**, *109*, 3637–3646.

(68) Jungkamp, T. P. W.; Smith, J. N.; Seinfeld, J. H. *J. Phys. Chem. A* **1997**, *101*, 4392–4401.

(69) Hayes, C. J.; Burgess, D. R. *Proceedings of Combustion Institute* **2009**, *32*, 263–270.

(70) Curran, H. J.; Gaffuri, P.; Pitz, W. J.; Westbrook, C. K. *Combust. Flame* **1998**, *114*, 149–177.

(71) Curran, H. J.; Gaffuri, P.; Pitz, W. J.; Westbrook, C. K. *Combust. Flame* **2002**, *129*, 253–280.